Anti-inflammatory drug diclofenac removal by a synthesized MgAl layered double hydroxide

H. Mkaddem [a,b,c], E. Rosales [a], M. Pazos [a], H. Ben Amor [c], M.A. Sanromán [a], J. Meijide [a,*]

[a] CINTECX, Universidade de Vigo, Grupo de Bioingeniería y Procesos Sostenibles, Departamento de Ingeniería Química, Campus Lagoas-Marcosende, 36310 Vigo, Spain
[b] University of Gabes, Faculty of Sciences of Gabe, 6072 Gabes, Tunisia
[c] University of Gabes, Engineering School (ENIG), RL Processes, Energetic, Environment, and Electric Systems, 6072 Gabes, Tunisia

ARTICLE INFO

ABSTRACT

Layered double hydroxides (LDHs) containing Mg:Al (molar ratio 3:1) were synthesized by co-precipitation from nitrate salts under alkaline conditions. Their further characterisation by different techniques allowed the determination of their structural, nanotextural and chemical properties. XRD measurements confirmed the high crystallisation with the presence of two metal cations (Mg^{2+} and Al^{3+}). The use of these materials as eco-friendly adsorbents was analysed to remove diclofenac from wastewater. Under optimal conditions (0.4 g L^{-1}, 30 ppm initial pollutant concentration, pH $\sim$ 8.5), around 65% diclofenac removal was achieved after 60 min of treatment. The pseudo-second kinetic order model and Freundlich isotherm accurately described the experimental data, suggesting chemisorption process on the heterogeneous LDH surface. After diclofenac adsorption, XRD analysis revealed an increase in interlayer spacing followed by contraction of adjacent layers, so that anion exchange between layer was considered to be the main mechanism for diclofenac adsorption. Thermodynamic studies indicate diclofenac adsorption occurs spontaneously, endothermically, and also, with increasing randomness at the solid/solution surface. Batch test revealed limitations in terms of long-term stability of the material. Therefore, a post-synthesis strategy, calcination, was required to increase the degree of resistance. For this purpose, the effect of calcination temperature was examined in the range 200–300 °C. Although, the kinetic rate constant decreased slightly after calcination, the improvement of its structural properties allowed to operate under continuous system.

© 2022 The Author(s). Published by Elsevier B.V. This is an open access article under the CC BY-NC-ND license (http://creativecommons.org/licenses/by-nc-nd/4.0/).

1. Introduction

Non-steroidal anti-inflammatory drugs (NSAIDs) such as paracetamol, ibuprofen, diclofenac and naproxen are widely used as analgesics, antipyretics, anti-inflammatories and anti-arthritics. Diclofenac, a known acidic non-biodegradable drug has been detected in hospital effluents and industrial wastewater at low concentrations ranging from sub-ng L^{-1} up to 19.82 mg L^{-1} [1]. Several authors have pointed out that wastewater treatment plants are the main contributors to the partial release into aquatic systems (e.g. maximum 21–40% diclofenac removal) [2,3].

In the literature, the removal of diclofenac from the aqueous phase has been investigated by many advanced oxidation processes, membrane filtration, and adsorption [4–8]. Cost-effective technologies mainly involve the use of materials from Earth-abundant elements with remarkable physicochemical properties (e.g., chemical stability, high adsorption activity) and wide applicability. Layered-double-hydroxides (LDHs) are anionic clays similar to brucite with good tuneability, high chemical stability, pH-dependent solubility and biocompatible material due to their flexible composition and anion exchangeability. The molecular formula of LDHs can be expressed as follows $[M_{1-x}^{2+} M_x^{3+} (OH)_2]^{x+}$ $(A^{m-})_{x/m} \cdot nH_2O$, where M^{2+} and M^{3+} are divalent and trivalent metal cations, respectively, A^{m-} is an interlayer anion and $\times$ is the molar ratio $[M^{3+}]/([M^{2+}] + [M^{3+}])$. The ratio of divalent to trivalent cations in the synthesis is between 2:1 to 4:1 since no LDH-based materials are formed below and above this threshold due to the high content of divalent and trivalent hydroxide, respectively. These hydrotalcites generally have an octahedral structure with the metal cations located in the centre of the angular unit and surrounded by six hydroxyl ions to form infinite layers [9].

LDH-based materials have been successfully used as catalysts and anion exchangers [10], as antacids agents and carriers for drug delivery carriers in medicine [11], in environmental remediation [12], as antimicrobial biomaterials, and for bio-sensing [9]. To date,

* Corresponding author.
  E-mail address: jmeijide@uvigo.es (J. Meijide).

few publications have investigated the use of these hydrotalcites as adsorbents for drug removal [13,14]. Unmodified LDHs usually show relatively low removal efficiency for many organic pollutants due to their limited functional group content [15]. In addition, aggregation of LDHs has a negative effect on the adsorption process due to deactivation of adsorption sites [16]. Post-synthesis strategies such as anion-exchange, rehydration, impregnation techniques and calcination have been successfully applied to obtain improved LDH-based materials [17]. Calcination is considered the most commonly used technique for thermal modification of LDH-based materials in terms of environmental aspects. Calcination temperatures above 500 °C promote the formation of highly crystalline metal oxides and spinel phases [18]. In contrast, calcination temperatures around 300 °C remove the interlayer anions and water molecules, leading to partial dehydroxylation of the LDH material and producing amorphous phases and slightly crystalline metal oxides on the structure.

Considering these conditions, the present research work focuses on diclofenac adsorption using MgAl LDH-based nanomaterial. After the synthesis, the material was characterised by analytical techniques to study its morphology, structure, chemical composition and thermal properties. In addition, batch adsorption experiments were performed to estimate the kinetic and equilibrium parameters using common empirical models. Subsequently, the synthesised materials were calcined at 200, 250 and 300 °C to evaluate their effect on diclofenac adsorption. Finally, column experiments were performed to investigate the effectiveness of MgAl-LDH as an adsorbent in environmental remediation.

2. Materials and methods

2.1. Reagents

The main properties of sodium diclofenac (≥99%, Sigma-Aldrich) used as the target pollutant are described in Table 1. Hydrotalcite was synthesised using magnesium nitrate hexahydrate (≥99%, VWR Group) and aluminium nitrate nonahydrate (≥99%, VWR Group) while sodium hydroxide (≥99%, Sigma-Aldrich) was used for pH adjustment. All reagents were used without purification and initial solutions were prepared using distilled water as solvent.

2.2. Synthesis of MgAl-NO$_3$ LDH

The LDH-based adsorbent was prepared using a co-precipitation method described elsewhere [19]. The synthesis of hydrotalcite Mg:Al (molar ratio 3:1) was carried out by dropwise addition of 100 mL of solution A containing magnesium (0.375 M) and aluminium (0.125 M) salts and 50 mL of solution B containing NaOH (2 M) into a three-neck flask containing 40 mL of distilled water at 65 °C with stirring. The pH of the solution was maintained at 10.5 during the synthesis process. Then, the slurry obtained was aged at 65 °C for 12 h with vigorous stirring. After the ageing step, the resulting precipitate was centrifuged at 6000 rpm for 5 min and washed with deionized water. The centrifugation-washing cycle was repeated several times until

the wash water achieved a neutral pH. The samples were then dried at 60 °C and grounded by hand with a mortar to obtain white powder.

2.3. Characterisation of MgAl-NO$_3$ LDH

2.3.1. Structural characterisation

The crystallite size was determined by X-ray diffraction (XRD) on a Siemens D5000 diffractometer (Bruker AXS Gmbh, Karlsruhe, Germany) using CuKα radiation with 2θ angle from 5 to 80° (CACTI, University of Vigo). The average crystallite size was estimated using the Scherrer's equation (Eq. (1)) [20].

$$D = \frac{0.89\lambda}{\beta \cos \theta_B} \tag{1}$$

where D is the average crystallite size (nm), λ is the wavelength of the X-rays (0.154 nm), β is the full-width at half-maximum intensity (FWHM), and θ_B is the half-diffraction angle (rad). The basal spacing and interlayer thickness were determined using Bragg's law (Eq. 2–3) [21].

$$d = \frac{\lambda}{2 \sin \theta_B} \tag{2}$$
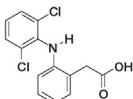
$$L = d - l \tag{3}$$

where d is the basal spacing (nm), λ is the wavelength of the X-rays (0.154 nm), θ_B is the half-diffraction angle (rad), l is the interlayer thickness (nm), and L is the layer thickness (nm). The thickness of brucite layer is around 0.477 nm [22].

The functional groups on the LDH surface were analysed by Fourier transform infrared spectroscopy (FTIR) at room temperature using Nicolet 6700 FT-IR spectrometers (Thermo Electron Corporation) in the range 4000–400 cm^{-1} with a resolution of 4 cm^{-1} and 34 scans (CACTI, University of Vigo). Sample spectra were recorded in KBr pellets containing 1 wt% of the material. Before preparing the KBr pellets, all samples and KBr were oven-dried overnight at 100 °C. Thermogravimetric analyses (TGA) were also performed to evaluate the thermal properties of the LDH using TG-DSC SETSYS Evolution 16/18 (Setaram, Caluire, France). All samples were heated to 800 °C at 10 °C/min under inert nitrogen flow (CACTI, University of Vigo).

2.3.2. Nanotextural and chemical characterisation

Nanotextural properties were analysed by recording the nitrogen adsorption isotherms at 196 °C (ASAP 2020 Plus, Micromeritics). Before injection, the samples were degassed under vacuum conditions at 200 °C (CACTI Ourense, University of Vigo). Determination of BET surface area, total pore volume and pore size were carried from the nitrogen adsorption data. BET surface area was calculated using the Brunauer-Emmett-Teller equation. Micropore volume was determined using the Dubinin-Radushkevich plot, while mesopore volume was estimated using the difference from total volume [23]. The morphological properties were studied using a field emission scanning electron microscope and energy-dispersive X-ray spectroscopy (FE-SEM/EDS) on a JEOL JSM 6700F

Table 1
Physicochemical properties of the diclofenac.

Pollutant	Structure	Molecular formula	Molecular weight (g mol^{-1})	Water solubility (mg mL^{-1})	pKa	log D
Diclofenac (NSAIDs)		C$_{14}$H$_{11}$Cl$_2$NO$_2$	296.1	296.15 (pH 8.5)	4.15	0.75 (pH 8.5)

(Japan) equipped with an energy dispersive X-ray spectrometer (EDS) and accelerating voltage of 20 kV (CACTI, University of Vigo). The point of zero charge of hydrotalcite (pH$_{PZC}$) was determined by the mass titration procedure as described elsewhere [24].

2.4. Experimental setup

Adsorption experiments were performed in batch by adding 20 mg LDH-based adsorbent to 50 mL of aqueous solution containing 30 mg/L of diclofenac. Samples were shaken using an orbital shaker (Thermo Scientific 420 Incubator Shaker) at 250 rpm and 25 °C. Aqueous samples were taken throughout the adsorption process to analyse kinetic and isothermal profiles. Diclofenac content was determined by spectrometric measurement at a fixed wavelength (λ = 275 nm). Before spectrophotometric analysis, all samples were filtered through 0.22 μm PVDF filters. As a post-synthesis strategy, the samples were calcined for 40 min at different temperatures (200, 250 and 300 °C) in a muffle furnace and then stored in a desiccator for cooling at room temperature. After the batch experiments, the presence of the anions (nitrate, nitrite, chloride) in the main solution was determined by ion chromatography, while the aluminium and magnesium concentrations were analysed by inductively coupled plasma (ICP-OES) (CACTI, University of Vigo).

2.5. Adsorption and isothermal kinetics

2.5.1. Adsorption kinetic models
The adsorption data obtained under non-equilibrium conditions have been described by two well-known empiric models, namely pseudo-first-order model (Eq. (4)) and pseudo-second-order model (Eq. (5)). Both of these equations were developed based on the concept of chemical reaction that occurs on the adsorbent surface [25]. The pseudo-second order model assumes that the rate-determining step is a chemical sorption or chemisorption between the adsorbent and adsorbate. Nevertheless, the pseudo-first order model suggests a physisorption process, which the rate-limiting stage is a diffusion step as a function of the concentration of the adsorbate [26].

$$q_t = q_e\left(1 - e^{-k_1 \cdot t}\right) \tag{4}$$

$$q_t = \frac{q_e^2 k_2 t}{1 + q_e k_2 t} \tag{5}$$

where q_t and q_e are the amount of adsorbed pollutant at time t and equilibrium (mg g^{-1}), respectively, and k_1 and k_2 are the equilibrium rate constants of pseudo-first order (min^{-1}) and pseudo-second order (g mg^{-1} min^{-1}), respectively.

2.5.2. Adsorption isothermal models
Several equilibrium isotherm models are used to describe the adsorption behaviour of the liquid solution on surface adsorbent. Among them, Langmuir (Eq.6) and Freundlich (Eq.7), two-parameter models are considered the most common isotherms to provide an understanding of the adsorption behaviour [27].

$$q_e = \frac{q_{max} b_L C_e}{1 + b_L C_e} \tag{6}$$

$$q_e = K_F C_e^{1/n} \tag{7}$$

where q_e is the equilibrium adsorbed amount (mg g^{-1}), C_e is the equilibrium concentration (mg L^{-1}), q_{max} is the maximum adsorbed amount (mg g^{-1}), b_L is the Langmuir equilibrium constant (L mg^{-1}), K_F is the Freundlich adsorption constant (L mg^{-1}) and n is an empirical constant related to the strength of the adsorption process.

Langmuir isotherm model assumes a monolayer process, which adsorption occurs only at homogeneous active sites with no lateral interaction between adsorbent molecules [28]. In contrast, the Freundlich isotherm suggests that the adsorption takes place by multilayer process on a heterogenous surface. In addition, the use of some three-parameter models has been successfully used on adsorption studies. In particular, Sips isotherm (Eq. (8)) is a hybrid model, which combine Langmuir and Freundlich isotherms assuming that the adsorption process occurs on heterogeneous surface and also, overcoming the limitation of the enhancement of the adsorbate concentration attributed to Freundlich isotherm.

$$q_e = \frac{K_S a_S C_e^{1/n}}{1 + a_S C_e^{1/n}} \tag{8}$$

where K_S (mg g^{-1}) and a_S (L$^{1/n}$ mg$^{-1/n}$) are the Sips isotherm model constants and n is the Sips isotherm model exponent.

2.6. Column adsorption system

Fixed-bed assays were performed by using a borosilicate Omnifit® glass column (10 cm long and 15 mm inner diameter) with calcined MgAl-LDH as filler and 20 μm PTFE frits as mechanical support layers. Continuous flow was introduced into the column by a peristaltic pump (Master Flex L/S model 77202–60). Experiments were performed at room temperature and the diclofenac concentration in the effluent was measured spectrometrically as described above (section 2.4).

2.7. Modelling of the breakthrough curves

2.7.1. Bed depth service time (BDST) model
The BDST model has been successfully used to describe and predict the performance of a dynamic adsorption system and for further scale-up. This model, developed by Hutchins and Anaya [29], shows a linear relationship between bed depth and operating time with negligible external film resistance and intraparticle mass transfer (Eq. (9)).

$$t = \frac{N_{BD}Z}{C_0 U_0} - \frac{1}{K_{BD}C_0} \ln\left(\frac{C_0}{C_t} - 1\right) \tag{9}$$

where C_0 and C_t are the initial and effluent concentrations of the solute in the liquid phase, respectively (mg L^{-1}), U_0 is the influent linear rate (cm s^{-1}), N_0 is the adsorption capacity (mg g^{-1}), k_a is the rate constant in the BDST model (L mg^{-1} s^{-1}), t is the time (s) and Z is the bed depth of the column (cm).

2.7.2. Yoon-Nelson model
The Yoon-Nelson model assumes that the decreasing rate for each adsorbate molecule depends on the probability of adsorption of the adsorbate and the breakthrough of the adsorbate on the adsorbent. The nonlinear form of the Yoon-Nelson model is given by Eq. (10) [30].

$$\frac{C}{C_0} = \frac{e^{(k_{YN}(t-\tau))}}{1 + e^{(k_{YN}(t-\tau))}} \tag{10}$$

where C_0 and C are the initial and effluent concentrations of the solute in the liquid phase, respectively (mg L^{-1}), t is the breakthrough time (min), K_{YN} is the rate constant (min^{-1}) and τ is the time required for 50% adsorbate breakthrough (min).

3. Results and discussion

3.1. Characterisation of the MgAl-NO₃ LDH

3.1.1. Structural characterisation

The hydrotalcite synthesised by co-precipitation exhibits a typical XRD pattern indexed by JCPDS 14–0191. The layered structure of the MgAl-LDH was confirmed by the presence of the symmetrical peaks at 2θ at 11.24°, 22.58°, 34.39°, 38.48°, 45.23°, 60.68° and 61.80°, respectively assigned to the planes (003), (006), (012), (015), (018), (110) and (113) [31–33]. Their high degree of crystallisation was confirmed by the sharp diffraction-peaks assigned to the (003) and (006) reflections, while the (110) and (113) planes correspond to a hexagonal lattice with rhombohedral R-3 m symmetry and the presence of two metal cations (Mg^{2+} and Al^{3+}) (Fig. 1a). The low intensity peaks around 2θ = 14.50°, 28.50° and 55.00° are attributed to the presence of AlOOH from parallel reactions between ionic hydroxide and excess Al [34]. The average crystallite size, unit cell dimensions, and cell volume are summarised in Table 2. The lattice constant corresponds to the average metal-metal spacing in the brucite-based layers estimated from the (110) reflection position, while the electrostatic interactions between the layers and the interlayer species calculated from the (003) reflection are defined by the parameter c [35]. Assuming a hexagonal unit cell structure, the basal spacing is related to the lattice parameters (a, c) and the Miller indices (hkl) (Eq. (11)).

$$\frac{1}{d^2} = \frac{4}{3}\left(\frac{h^2 + hk + k^2}{a^2}\right) + \frac{l^2}{c^2} \tag{11}$$

In addition, the volume cell was determined from the unit cell parameters assuming the hexagonal packing of the MgAl-LDH structure [36]. The basal spacing, d, was estimated from the first peak in the XRD pattern using Bragg's law (Eq. (2)) from interlayer spacing, being 7.87 Å. These results are in agreement with those of de Souza dos Santos et al. [13], who had previously determined the mean basal spacing for MgAl-LDH. The crystallite size of the MgAl-LDH was calculated using the Scherrer's equation (Eq. (1)), and yielded D values around 0.86 nm. The FTIR spectrum of the synthesised MgAl-LDH (Fig. 1c) showed some characteristic peaks previously reported in the literature [37–39]. The broader bands around 3400 cm^{-1} and 1630 cm^{-1} correspond to the O-H stretching in the brucite-based layers $Mg(OH)_2$ and $Al(OH)_3$ and the bending vibrations of the hydroxyl groups as a result of the intermolecular water molecules, respectively. The band corresponding to the antisymmetric stretching vibration mode of the nitrate ions is located at 1350 cm^{-1}, while the peaks below than 1000 cm^{-1} can be attributed to the Mg-O and Al-O lattice vibrations [39]. Moreover, the band at 1360 cm^{-1} is characteristic of the carbonate ions of CO_2 dissolved in water [38].

The thermal stability of hydrotalcite was investigated by TGA measurements. Three distinguishable regions associated with the temperature range from 20 to 250 °C, 250–415 °C and 415–800 °C can be seen in Fig. 1d. Around 15% mass loss at temperatures below 250 °C is probably due to the removal of physisorbed water and water from the interlayers of the LDH structure [40]. Dehydroxylation of MgAl-LDH and release of carbonate ions from the interlayer occurs to a lesser extent at 300 °C, resulting in remarkable percent mass loss (~35%). Above 400 °C, the collapse
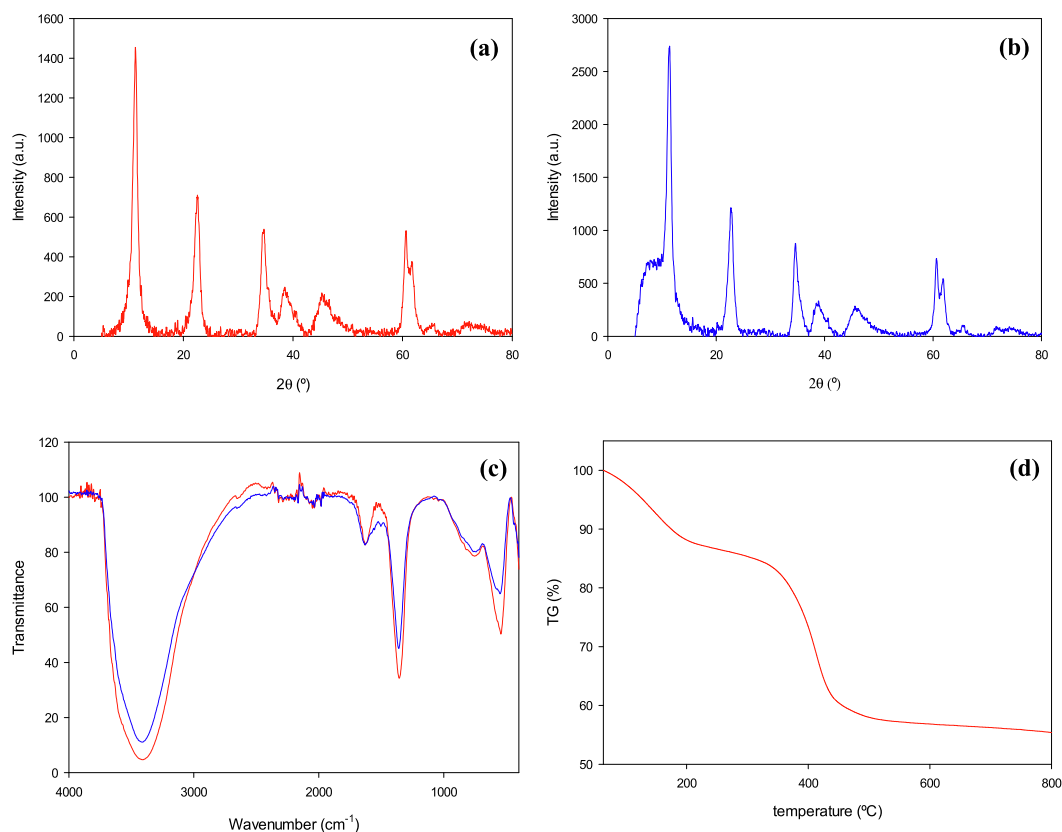

Fig. 1. XRD spectra of MgAl-LDH (a) before and (b) after diclofenac adsorption, (c) FT-IR spectra of MgAl-LDH before (red line) and after (blue line) diclofenac adsorption and (d) TGA profile of raw MgAl-LDH.

Table 2

Structural and nanotextural properties of the crystal MgAl-LDH.

Sample	Unit cell parameters[a]			Crystallite size[b] (Å)				Surface area[c] (m^2 g^{-1})	Pore volume[c] (cm^3 g^{-1})	Average pore diameter[c] (Å)
	a (Å)	c (Å)	V (Å^3)	D$_{003}$	L$_{003}$	D$_{110}$	L$_{003}$			
MgAl-LDH	3.05	23.59	190.0	8.64	3.84	6.31	1.54	4.49	0.0096	85.6
MgAl-LDH (250 °C)	5.19	23.56	549.6	7.56	2.76	6.30	1.50	2.23	0.0059	105.2

[a] a = 2 d(1 1 0), c = 3 d(0 0 3), V = $\sqrt{3}$ a^2 c/2.
[b] Estimation by Debye-Scherrer's and Bragg's equations.
[c] Estimation by BET analysis.

of the MgAl-LDH structure results in the formation of metal oxides such as MgO and MgAl$_2$O$_4$ and a spinel structure [13].

3.1.2. Nanotextural characterisation

The morphology of the synthesised LDH crystal was observed from FE-SEM microscopic graphs. On a high magnification FE-SEM image (Fig. 2a, 2b), MgAl-LDH shows a hierarchical 3-D structure consisting of many randomly oriented 2D-nanosheets that produce a smooth surface. These nanoflower-like structures were built by the abundant intercalated nanoplatelets, which provide notable specific surface area with numerous microporous within the perfect lamellar structure, confirming the results of XRD analysis [35]. No dark areas in the FE-SEM images are detected showing negligible tendency of the particles to agglomerate into aggregated crystallites. From this analysis, the average thickness of the platelet-like particles was around 30–40 nm. In addition, FE-SEM/EDS analysis showed that carbon, oxygen, nitrogen, magnesium and aluminium were uniformly distributed throughout the material, confirming the successful synthesis process. No other peaks were detected, indicating the high purity of these materials (Fig. 2c). From the EDS spectra, the Mg/Al molar ratio was around 3:1 as the precursor-feed ratio. Nitrogen adsorption analysis was performed to estimate the surface properties listed in Table 2, such as specific surface area, pore size distribution, and pore volume. As shown in Fig. 2d, nitrogen adsorption resulted in a type IV pattern according to the IUPAC classification with a closed H$_3$-type hysteresis loop at high relative pressure. The material exhibits the characteristic property of a mesoporous solid with pore sizes ranging from 2 to 50 nm. The pronounced hysteresis loop was attributed to capillary condensation that occurred in the mesopores, while the shape and position of the loop depended on the morphology of the solid (specific pore structures and degree of compaction) [13]. The amphoteric character of MgAl-LDH was demonstrated by estimating pH$_{PZC}$ over a pH range 2.5–10.5 (Fig. 3a). Based on these results, pH$_{PZC}$ corresponds to a slightly alkaline pH (around 8.7). This fact reflects the potential of the synthesised LDH as an adsor-
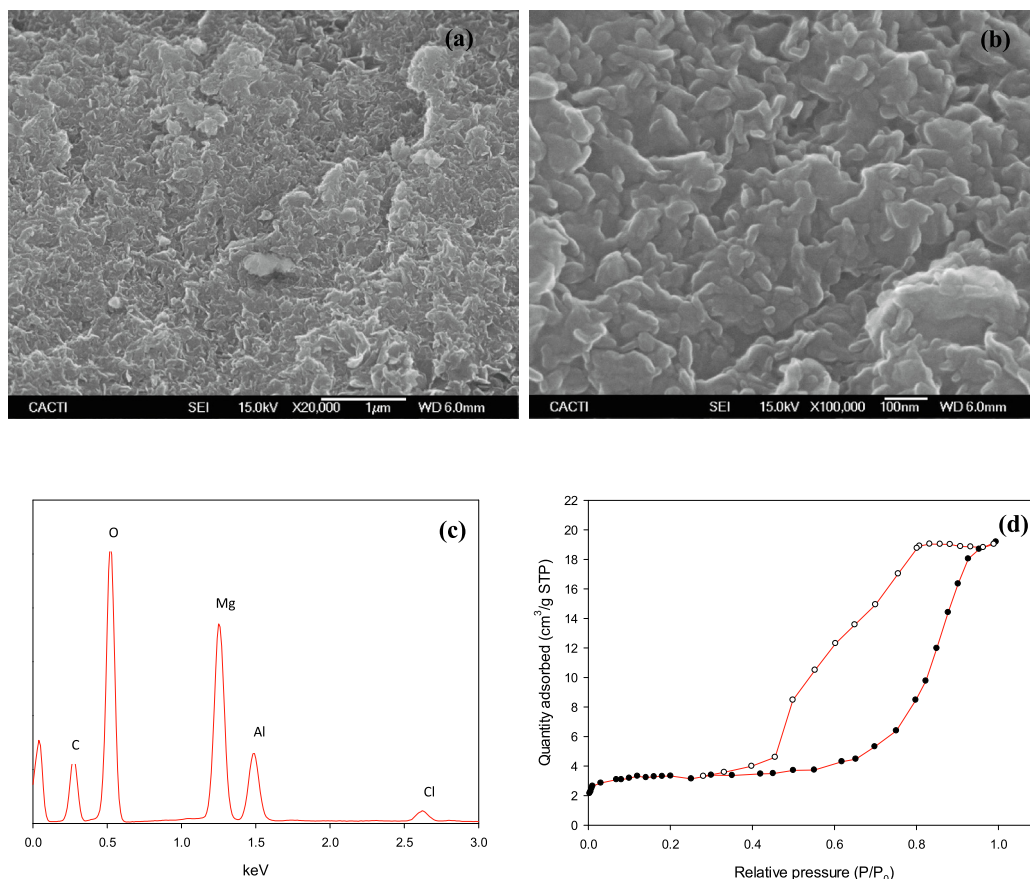

Fig. 2. FE-SEM micrographs of the MgAl-NO$_3$ LDH (a,b:20,000X, 100,000X), (c) Elemental composition from EDS results of raw MgAl-NO$_3$ LDH and (d) surface area measurements for raw MgAl-NO$_3$ LDH using nitrogen adsorption–desorption isotherms.
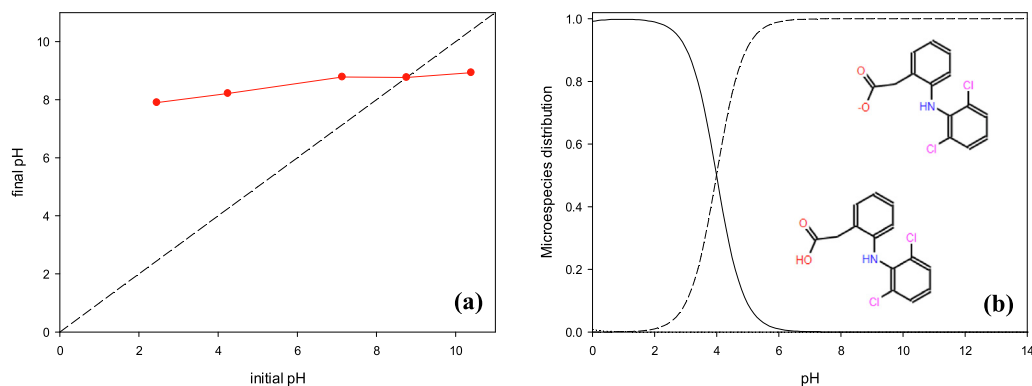
Fig. 3. Determination of the point of zero charge (pH$_{PZC}$) (a) Speciation of the diclofenac as a pH-dependent (b).

bent. Adsorption of anionic species is promoted at pH below pH$_{PZC}$ (positive surface charge), while adsorption of cationic species is favoured at pH above pH$_{PZC}$ (negative surface charge).

3.2. Effect of pH on diclofenac adsorption

Solution pH is a key parameter for the adsorption of ionisable pharmaceuticals controlling the interfaces between water and adsorbent [41]. The adsorption of diclofenac was inhibited at pH below pK$_a$ because the water solubility of the pollutant decreases, leading to its further precipitation [42,43]. The pH-dependent speciation of diclofenac can be seen in Fig. 3b. The major fraction of anionic species at pH above 4.5 promotes the adsorption process, as most of the reported pH$_{PZC}$ of LDHs are in the range of 7–8 [24,44]. Hydrotalcites are positively charged at a pH below the pH$_{PZC}$, which promotes the adsorption of anionic species, while a negative charge at a pH above the pH$_{PZC}$ promotes the adsorption of cationic species [45]. Similarly, previous publications have shown the release of metal cations from the LDH material at a pH below 4, leading to the formation of magnesium and aluminium hydroxides [46,47]. Therefore, the effectiveness of the process was analysed at pH values between 7 and 12. The adsorption capacity of the hydrotalcite was improved by increasing the pH up to 8.5; nevertheless, pH values above this threshold have a negative effect on the removal of diclofenac. The adsorption capacity decreased in an alkaline medium (pH around 12) due to the repulsive electrostatic interaction between the anionic species of the target pollutant and the negative charge on the adsorbent surface. These results are in agreement with those of Li et al. [24], who evaluated the potential use of hydrotalcite for the removal of tetracycline and sodium diclofenac from an aqueous solution. The authors reported a maximum adsorption capacity around 890 mg g^{-1} and 270 mg g^{-1} for tetracycline and sodium diclofenac, respectively. Based on these considerations, electrostatic interactions could be one of the main driving forces for adsorption.

3.3. Kinetic, isothermal and thermodynamic studies of adsorption

3.3.1. Kinetic and isothermal studies on diclofenac adsorption by MgAl-NO₃

The kinetic studies were investigated using pseudo-first and pseudo-second order kinetic models (Eq.4–5) to determine the interactions between adsorbate and adsorbent [25,48]. The kinetic parameters are listed in Table 3. Higher correlation coefficients and similar theoretical and experimental uptake from the pseudo-second order showed chemisorption as the dominant process. These results are in agreement with those of Xu et al. [39], who also confirmed the chemisorption mechanism using the Elovich

model. No diffraction-angle peaks corresponding to the diclofenac were observed from the post-adsorption spectrum (Fig. 1b). However, slight shifts in the reflections were detected, which increased the basal spacing and confirmed the replacement of interlayer anions by anionic pollutants in the bulk solution [49]. Three peaks at (0 0 3) position showed an increase in the interlayer distance followed by contraction of the adjacent layers [50]. Therefore, the interlayer anion exchange is probably the most important mechanism in the adsorption. These results are consistent with the remarkable release of nitrate ions (around 45% initial NO₃ concentration) into the solution after adsorption of diclofenac, confirming anionic exchange as the main mechanism for pollutant removal. In addition, the chloride ion concentration after diclofenac adsorption was analysed by chromatographic techniques, and negligible chloride content was found in the aqueous phase. The FTIR spectrum of diclofenac was previously reported by Zhao et al. [51] and Younes et al. [14], who detected some characteristic bands situated at 3388 cm^{-1} (ν_{N-H}), 3257 cm^{-1} ($\nu_{N-H\cdots O}$ due to the intermolecular hydrogen bonding), 3077 cm^{-1} ($\nu_{C-H, \text{ aromatic}}$), 1571 cm^{-1} ($\nu_{COO-, \text{ antisymmetric}}$), 1503 cm^{-1} ($\nu_{C=C, \text{ aromatic}}$), 1450 cm^{-1} ($\nu_{COO-, \text{ symmetric}}$), 1289 cm^{-1} ($\nu_{C-N, \text{ aromatic}}$), 748 cm^{-1} ($\delta_{C-H, \text{ aromatic}}$) and 448 cm^{-1} ($\nu_{C-Cl}$). The FTIR analysis after adsorption provided information about the effectiveness of the process. It showed that the chemical structure of hydrotalcite did not exhibit any remarkable changes after adsorption (Fig. 1c), and thus, the anion exchange reaction was the main mechanism, as indicated by the XRD patterns. The low diclofenac concentration hinders the detection of its characteristic band; indeed, only a weak band at 1571 cm^{-1} was assigned to the antisymmetric stretching vibration of the carbonyl groups of diclofenac. Before adsorption, the intensity of this peak was slightly higher than the band at 1450 cm^{-1} assigned to the symmetric stretching vibration. Nevertheless, this trend reversed after the sorption process, indicating that the oxygen atoms of the –COOH group contributed to the removal of diclofenac from the aqueous phase by metal complexation [14,37]. Moreover, the fluctuation detected in the band around 3400 cm^{-1} was attributed to the O-H vibration due to the formation of H-bonds between the hydrogen acceptors of the diclofenac structure (–NH, –COO– and Cl-) and the hydrogen donors of the MgAl-LDH (–OH groups).

In addition, the experimental data from the equilibrium studies were analysed using empirical models with two- and three-parameters such as Langmuir, Freundlich and Sips models. Among the equilibrium constants listed in Table 4, the two-parameter models showed higher correlation coefficients and lower SEE, confirming their authenticity. The Freundlich model describes the adsorption of diclofenac on the heterogeneous adsorbent surfaces at relatively high adsorbate concentrations. These materials have heterogeneous surfaces, as observed by SEM microscopic images,

Table 3

Kinetic parameters for different models on diclofenac adsorption using LDH-based materials.

Hydrotalcites	$q_{e, exp}$ (mg g^{-1})	Pseudo-first order			Pseudo-second order			Reference
		q_e (mg g^{-1})	k_1 (min^{-1})	R^2	q_e (mg g^{-1})	k_2 (g mg^{-1} min^{-1})	R^2	
MgAl-LDH	60.15	49.78	0.028	0.951	65.47	0.001	0.985	This study
MgAl-LDH (200 °C)	48.78	44.07	0.119	0.934	48.90	0.003	0.981	This study
MgAl-LDH (250 °C)	41.30	33.29	0.122	0.885	36.27	0.005	0.949	This study
MgAl-LDH (300 °C)	40.38	30.92	0.036	0.814	35.08	0.001	0.914	This study
MgAl-LDH	40.00	39.11	n.a.	0.985	43.46	n.a.	0.995	[13]
MgAl-LDH-biochar	35.00	33.03	n.a.	0.969	39.46	n.a.	0.985	[13]
ZnFe-LDH	14.66	13.84	1.080	0.860	14.44	0.100	0.990	[14]

n.a.: not available.

Table 4

Isotherm parameters for different models on diclofenac adsorption using LDH-based materials.

Models	MgAl-LDH		MgAl-LDH (250 °C)	
Langmuir	q_{max} (mg g^{-1})	76.93	q_{max} (mg g^{-1})	173.9
	b_L (L mg^{-1})	0.076	b_L (L mg^{-1})	0.079
	R^2	0.919	R^2	0.895
	SEE (mg g^{-1})	5.773	SEE (mg g^{-1})	55.05
Freundlich	K_F (mg$^{(n+1)/n}$ g^{-1} L$^{-1/n}$)	9.380	K_F (mg$^{(n+1)/n}$ g^{-1} L$^{-1/n}$)	17.12
	n	1.857	N	1.604
	R^2	0.935	R^2	0.942
	SEE (mg g^{-1})	5.182	SEE (mg g^{-1})	10.83
Sips	q_s (mg g^{-1})	71.99	q_s (mg g^{-1})	108.1
	a_s (L$^{1/n}$ mg$^{-1/n}$)	0.522	a_s (L$^{1/n}$ mg$^{-1/n}$)	0.053
	n	1.857	N	1.838
	R^2	0.947	R^2	0.902
	SEE (mg g^{-1})	17.08	SEE (mg g^{-1})	23.71

providing all the theoretical properties obtained by the isotherms. Their maximum adsorption capacity was about 60 mg g^{-1}, a higher adsorption uptake compared to other publications in the literature on the removal of diclofenac from aqueous phase (Table 3) [13,14,52].

3.3.2. Thermodynamic analysis

Thermodynamic analysis was performed to determine the effect of temperature on the adsorption process (Fig. S1) [17,53]. For this purpose, three general thermodynamic parameters such as standard Gibbs free energy ($\Delta G°$), standard enthalpy ($\Delta H°$) and standard entropy ($\Delta S°$) were estimated using Eq. 12–14 [54].

$$\Delta G° = \Delta H° - T\Delta S° \tag{12}$$

$$\Delta G° = -RT \ln K \tag{13}$$

$$\ln K = \frac{-\Delta H°}{RT} + \frac{\Delta S°}{R} \tag{14}$$

where K is the equilibrium constant value, R is the universal gas constant (8.314 J mol^{-1} K^{-1}) and T is the absolute temperature (K).

High temperatures slightly increase the adsorption efficiency, indicating the diclofenac adsorption is an endothermic adsorption process, which is consistent with the estimated thermodynamic parameters [55]. The physisorption mechanism generally involves $\Delta H°$ values ranging from 5 to 40 kJ mol^{-1} while $\Delta H°$ values above this threshold correspond to the chemisorption mechanism [56]. These results are consistent with the kinetic studies previously analysed in subsection 3.3.1, where the authors described the pseudo-second order as the most appropriate empirical model to fit the experimental data. A negative $\Delta G°$ value means the diclofenac adsorption process was thermodynamically spontaneous and favourable. A positive $\Delta S°$ value provides relevant information about the increasing randomness at the solid/solution surface and indicates that the adsorption process involves dissociative

mechanisms and therefore, this phenomenon is not favourable at high temperatures [57]. These magnitudes are listed in Table 5. The apparent activation energy, E_a was calculated according to Arrhenius' law (Eq. (15)) [58].

$$k = Ae^{\frac{-E_a}{RT}} \tag{15}$$

where k is the pseudo-second order kinetic constant (g mg^{-1} min^{-1}), A is the frequency factor, R is the universal gas constant (8.314 J mol^{-1} K^{-1}) and T is the absolute temperature (K).

For this purpose, the kinetic rate constants for diclofenac adsorption at different temperatures were determined by fitting the experimental data to the pseudo-second order kinetic model. The values of 2.56·10^{-4}, 5.24·10^{-4} and 5.88·10^{-4} g mg^{-1} min^{-1} were obtained for 298, 303 and 308 K, respectively. The apparent activation energy was determined by plotting ln k versus 1/T. Higher E_a values were obtained, confirming the chemical adsorption process and stronger forces compared to physical adsorption [58].

3.4. Thermal modification of the adsorbent

Previous studies have reported the improvement of adsorption process for anionic pollutants after calcination treatment [14,36,59] and consequently, LDH structures are reconstituted after hydration due to the "structural memory effect" [60]. Moreover, calcination of such materials especially promotes the formation of mixed oxides, which increase the specific surface area and the number of basic active sites. Therefore, the effect of calcination temperature ranging from 200 to 300 °C on the diclofenac adsorption process was studied. At temperature below 250 °C, high structural instability of these materials was found due to incomplete removal of physisorbed and interlayer water from the LDH structure, resulting in continuous release of adsorbed pollutant, while calcination temperatures above 300 °C caused the breakdown of the structure. The kinetic adsorption rate constants decreased

Table 5
Thermodynamic study of the diclofenac adsorption on the MgAl-LDH.

ΔG° (kJ mol^{-1})			ΔH° (kJ mol^{-1})	ΔS° (J mol^{-1} K^{-1})	E_a (kJ mol^{-1})	A (min^{-1})
298 K	308 K	318 K				
−6.746	−7.794	−8.843	55.76	209.7	63.61	$3.99 \cdot 10^7$

slightly after the calcination step; nevertheless, the structural stability of the calcined material improved significantly allowing it to operate under a continuous system. As shown in Fig. 4, the concentration profiles showed two distinct sections due to the adsorption process of the diclofenac on LDH (fast step) and the phenomenon of further reconstruction (slow step). These results are in agreement with those of Elhalil et al. [36], who studied the influence of the molar ratio and calcination temperature of ZnAl-LDH on the drug removal.

The experimental data were accurately described by the pseudo-second kinetic order model and Freundlich isotherm, as summarised in Tables 3-4. Based on the above premises, the optimum calcination temperature of 250 °C was used for the synthesised material packed on the column adsorption system.

After calcination, the broadening and weakening of the XRD pattern showed the decrease of the degree of crystallinity due to the formation of partially mixed metal oxide. As expected, the lamellar structure collapsed, leading to the formation of MgO-periclase-solid solution (JCPDS 45–0946), whose chemical structure exhibits cation vacancies due to the incorporation of trivalent cations into octahedral sites [61]. The average crystallite size, unit cell dimensions and cell volume for the calcined material are summarised in Table 2. The FT-IR spectra of the calcined samples showed a significant decrease in the intensity of the bands associated with the O-H groups, indicating dehydroxylation of LDH. The release of the low content of carbonate ions from the interlayer space was associated with the low intensity of the band assigned the stretching vibration of carbonate ions (around 1368 cm^{-1}). The FT-IR spectra showed an increasing intensity of the band corresponding to the lattice vibration Mg-O, and located in the low-frequency region ($\sim$600 cm^{-1}). The pore properties and surface area of the calcined material were tested by nitrogen adsorption-desorption isotherms. The calcined material has all the relevant characteristics of a mesoporous solid, as the specific surface area of LDH increases slightly after the calcination step (Table 2).

3.5. Column adsorption system

The behaviour of the dynamic adsorption system was analysed using a fixed-bed column (Fig. 5). The adsorbed total mass can be estimated from the area under the plot C_0-C_t vs. time using the Eq. (16), while the experimental equilibrium capacity was determined by Eq. (17) [62,63].

$$m_{total} = \int_0^t F(C_0 - C_t) \tag{16}$$

$$q_{e(exp)} = \frac{m_{total}}{M} \tag{17}$$

where m_{total} is the adsorbed total mass (mg), C_0 and C_t are the initial concentration and concentration at time t, respectively (mg L^{-1}), F is the flow rate (mL min^{-1}), t is the total time (min), $q_{e\,(exp)}$ is the equilibrium capacity (mg g^{-1}) and M is the total adsorbent mass packed within the column (g).

The dynamic system showed that the experimental equilibrium capacity determined by Eq. (17) was around 201 mg g^{-1}, which is consistent with the batch experiments results (Table 4). An appropriate design of the column requires an analysis of the fixed-bed behaviour using the empirical models such as the BDST and Yoon–Nelson models.
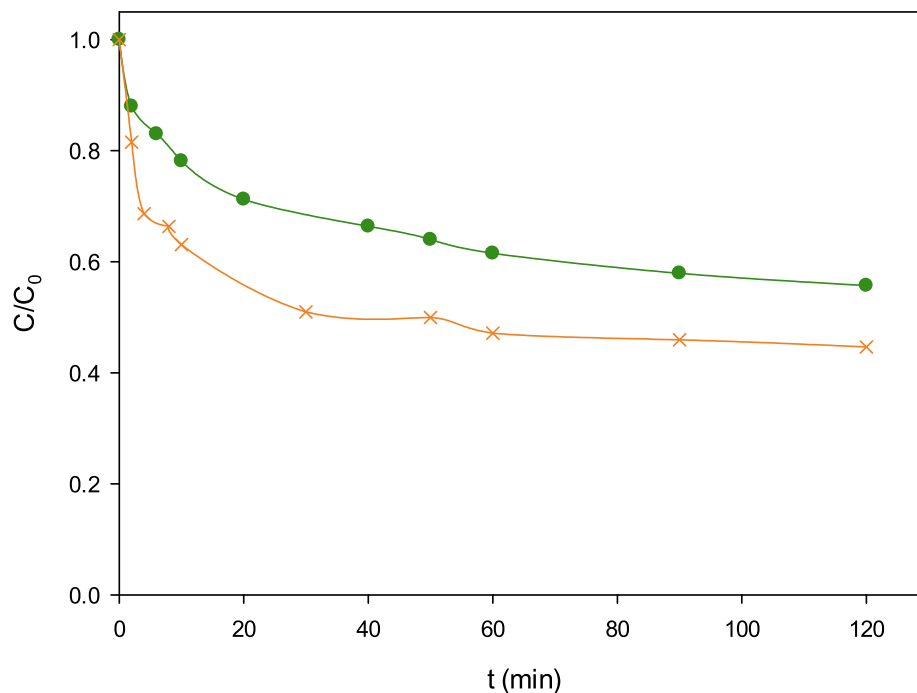

Fig. 4. Effect of the calcination temperature on the diclofenac adsorption using MgAl-NO$_3$ LDH: (dark green thin x) 250 °C, (orange circle) 300 °C.
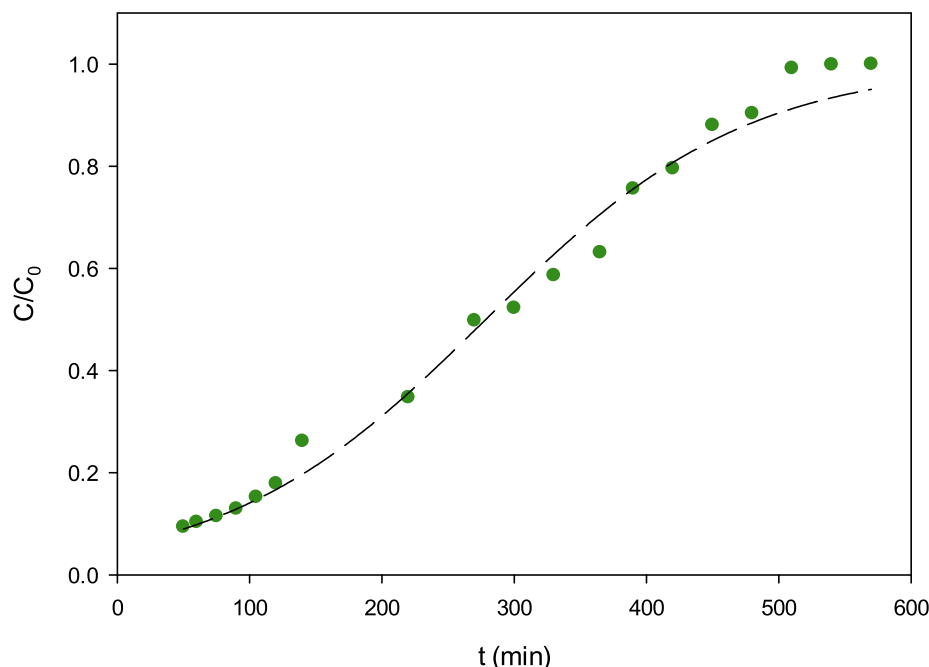
Fig. 5. Breakthrough curves for diclofenac adsorption on calcined MgAl-LDH fixed-bed column.

The linear representation of the BDST model (t *vs* ln (C_0 /C_t −1) allowed the determination of the BDST parameters (N_{BD} and K_{BD}) based on the slope and intercept. These parameters are listed in Table 6. A relatively high N_{BD} parameter implies a remarkable adsorption performance of the MgAl-NO_3 LDH for the removal of diclofenac from an aqueous solution. From the low-rate constant resulting from the BDST model, the authors inferred a low mass transfer from the liquid to the solid phase. The relatively high correlation coefficient of this model indicates that the main driving force of the process corresponds to the concentration gradient. Therefore, the available active sites decrease sharply at high pollutant concentration, leading to a decrease in breakthrough time and saturation time.

From nonlinear plot of the Yoon-Nelson model (C_t/(C_0-C_t) *vs* t), the time required for 50% adsorbate breakthrough was estimated to be about 270 min. Thus, the theoretical value agrees with the experimental value. The nonlinear models accurately described the experimental data from the dynamic system with a high correlation coefficient and low SEE values (Table 6).

4. Conclusions

The presence of two metal cations with a molar ratio of Mg:Al molar around 3:1 proved the successful synthesis of MgAl-LDH by coprecipitation. After the successful synthesis, the adsorption capacity of these materials was analysed with diclofenac as a model drug. Under optimal conditions, the removal of this anti-inflammatory compound (70 mg g^{-1} adsorptive capacity) was accurately described by the pseudo-second kinetic order model and Freundlich isotherm, indicating chemisorption as one of the main processes on the heterogeneous adsorbent surface. Then, a thermal treatment at 250 °C allowed to increase the structural stability of the material for operating in continuous flow. The dynamic system exhibited the experimental equilibrium capacity of the calcined material was around 201 mg g^{-1}, which is consistent with the batch experiments results. Thus, layered double hydroxides can be considered as promising materials for the search and development of novel adsorbents for wastewater treatment. Further studies are needed to investigate the presence of other inorganic ions and other emerging pollutants and the water matrix (e.g., municipal wastewater, hospital effluents) to demonstrate the general applicability of the proposed method.

Table 6
Operational conditions of the dynamic system and the estimated parameters for the BDST and Yoon-Nelson models.

Operational parameters	
Q (mL min^{-1})	1.00
m (g)	0.40
q_e (mg g^{-1})	201
Bed height (cm)	1.00
Breakthrough time (min)	60
Exhaustion time (min)	480
BDST model	
N_{BD} (mg g^{-1})	$1.34·10^3$
K_{BD} (L mg^{-1} s^{-1})	$1.58·10^{-4}$
R^2	0.8503
SEE (min)	67.65
Yoon-Nelson model	
k_{YN} (min^{-1})	0.0101
τ (min)	278.5
R^2	0.9871
SEE	0.0402

CRediT authorship contribution statement

H. Mkaddem: Methodology, Data curation, Writing – review & editing. **E. Rosales:** Investigation, Validation, Data curation, Writing – review & editing. **M. Pazos:** Conceptualization, Funding acquisition, Project administration, Writing – review & editing. **H. Ben Amor:** Writing – review & editing. **M.A. Sanromán:** Conceptualization, Funding acquisition, Project administration, Writing – review & editing. **J. Meijide:** Conceptualization, Investigation, Validation, Data curation, Writing – original draft, Writing – review & editing.

Declaration of Competing Interest

Acknowledgements

Appendix A. Supplementary material

Supplementary data to this article can be found online at https://doi.org/10.1016/j.molliq.2022.119207.

References

[1] Y. Vieira, H.A. Pereira, J. Leichtweis, C.M. Mistura, E.L. Foletto, L.F.S. Oliveira, G. L. Dotto, Effective treatment of hospital wastewater with high-concentration diclofenac and ibuprofen using a promising technology based on degradation reaction catalyzed by Fe0 under microwave irradiation, Science of The Total Environment 783 (2021) 146991, https://doi.org/10.1016/j.scitotenv.2021.146991.

[2] S.F. Soares, T. Fernandes, M. Sacramento, T. Trindade, A.L. Daniel-da-Silva, Magnetic quaternary chitosan hybrid nanoparticles for the efficient uptake of diclofenac from water, Carbohydrate Polymers 203 (2019) 35–44, https://doi.org/10.1016/j.carbpol.2018.09.030.

[3] Y. Zhang, S.U. Geißen, C. Gal, Carbamazepine and diclofenac: Removal in wastewater treatment plants and occurrence in water bodies, Chemosphere 73 (2008) 1151–1161, https://doi.org/10.1016/J.CHEMOSPHERE.2008.07.086.

[4] P.V.S. Lins, D.C. Henrique, A.H. Ide, J.L. da silva Duarte, G.L. Dotto, A. Yazidi, L. Sellaoui, A. Erto, C.L. de P. e S. Zanta, L. Meili, Adsorption of a non-steroidal anti-inflammatory drug onto MgAl/LDH-activated carbon composite – Experimental investigation and statistical physics modeling, Colloids and Surfaces A: Physicochemical and Engineering Aspects. 586 (2020) 124217, doi: https://doi.org/10.1016/j.colsurfa.2019.124217.

[5] R. Zhuan, J. Wang, Degradation of diclofenac in aqueous solution by ionizing radiation in the presence of humic acid, Separ. Purif. Technol. 234 (2020), https://doi.org/10.1016/J.SEPPUR.2019.116079 116079.

[6] S. He, J. Wang, L. Ye, Y. Zhang, J. Yu, Removal of diclofenac from surface water by electron beam irradiation combined with a biological aerated filter, Radiat. Phys. Chem. 105 (2014) 104–108, https://doi.org/10.1016/J.RADPHYSCHEM.2014.05.019.

[7] S. Zhuang, R. Cheng, J. Wang, Adsorption of diclofenac from aqueous solution using UiO-66-type metal-organic frameworks, Chem. Eng. J. 359 (2019) 354–362, https://doi.org/10.1016/J.CEJ.2018.11.150.

[8] S. Zhuang, Y. Liu, J. Wang, Mechanistic insight into the adsorption of diclofenac by MIL-100: experiments and theoretical calculations, Environ. Pollut. 253 (2019) 616–624, https://doi.org/10.1016/J.ENVPOL.2019.07.069.

[9] G. Mishra, B. Dash, S. Pandey, Layered double hydroxides: a brief review from fundamentals to application as evolving biomaterials, Appl. Clay Sci. 153 (2018) 172–186, https://doi.org/10.1016/J.CLAY.2017.12.021.

[10] G. Fan, F. Li, D.G. Evans, X. Duan, Catalytic applications of layered double hydroxides: recent advances and perspectives, Chem. Soc. Rev. 43 (2014) 7040–7066, https://doi.org/10.1039/C4CS00160E.

[11] V. Rives, M. del Arco, C. Martín, Intercalation of drugs in layered double hydroxides and their controlled release: a review, Appl. Clay Sci. 88–89 (2014) 239–269, https://doi.org/10.1016/J.CLAY.2013.12.002.

[12] K. Watson, M.J. Farré, N. Knight, Strategies for the removal of halides from drinking water sources, and their applicability in disinfection by-product minimisation: a critical review, J. Environ. Manage. 110 (2012) 276–298, https://doi.org/10.1016/j.jenvman.2012.05.023.

[13] G.E. de Souza, A.H. dos Santos, J.L.S. Ide, G. Duarte, A.O.S. McKay, L.M. Silva, Adsorption of anti-inflammatory drug diclofenac by MgAl/layered double hydroxide supported on Syagrus coronata biochar, Powder Technol. 364 (2020) 229–240, https://doi.org/10.1016/j.powtec.2020.01.083.

[14] H.A. Younes, R. Khaled, H.M. Mahmoud, H.F. Nassar, M.M. Abdelrahman, F.I. Abo El-Ela, M. Taha, Computational and experimental studies on the efficient removal of diclofenac from water using ZnFe-layered double hydroxide as an environmentally benign absorbent, Journal of the Taiwan Institute of Chemical Engineers 102 (2019) 297–311, https://doi.org/10.1016/j.jtice.2019.06.018.

[15] D. Yang, X. Wang, N. Wang, G. Zhao, G. Song, D. Chen, Y. Liang, T. Wen, H. Wang, T. Hayat, A. Alsaedi, X. Wang, S. Wang, In-situ growth of hierarchical layered double hydroxide on polydopamine-encapsulated hollow Fe3O4 microspheres for efficient removal and recovery of U(VI), J. Clean. Prod. 172 (2018) 2033–2044, https://doi.org/10.1016/J.JCLEPRO.2017.11.219.

[16] Y. Wang, Y. Gu, D. Xie, W. Qin, H. Zhang, G. Wang, Y. Zhang, H. Zhao, A hierarchical hybrid monolith: MoS42--intercalated NiFe layered double hydroxide nanosheet arrays assembled on carbon foam for highly efficient heavy metal removal, J. Mater. Chem. A 7 (2019) 12869–12881, https://doi.org/10.1039/C9TA03102B.

[17] K. Nava-Andrade, G.G. Carbajal-Arízaga, S. Obregón, V. Rodríguez-González, Layered double hydroxides and related hybrid materials for removal of pharmaceutical pollutants from water, J. Environ. Manage. 288 (2021), https://doi.org/10.1016/J.JENVMAN.2021.112399 112399.

[18] G. Mascolo, M.C. Mascolo, On the synthesis of layered double hydroxides (LDHs) by reconstruction method based on the "memory effect", Micropor. Mesopor. Mater. 214 (2015) 246–248, https://doi.org/10.1016/J.MICROMESO.2015.03.024.

[19] J. Inacio, C. Taviot-Guého, C. Forano, J.P. Besse, Adsorption of MCPA pesticide by MgAl-layered double hydroxides, Appl. Clay Sci. 18 (2001) 255–264, https://doi.org/10.1016/S0169-1317(01)00029-1.

[20] A.L. Patterson, The Scherrer formula for X-ray particle size determination, Phys. Rev. 56 (1939) 978–982, https://doi.org/10.1103/PhysRev.56.978.

[21] E. Alibakhshi, E. Ghasemi, M. Mahdavian, B. Ramezanzadeh, S. Farashi, Active corrosion protection of Mg-Al-PO43− LDH nanoparticle in silane primer coated with epoxy on mild steel, J. Taiwan Inst. Chem. Eng. 75 (2017) 248–262, https://doi.org/10.1016/J.JTICE.2017.03.010.

[22] J. Tedim, S.K. Poznyak, A. Kuznetsova, D. Raps, T. Hack, M.L. Zheludkevich, M.G. S. Ferreira, Enhancement of active corrosion protection via combination of inhibitor-loaded nanocontainers, ACS Appl. Mater. Interfaces 2 (2010) 1528–1535, https://doi.org/10.1021/am100174t.

[23] L.P. Bakos, J. Mensah, K. László, T. Igricz, I.M. Szilágyi, Preparation and characterization of a nitrogen-doped mesoporous carbon aerogel and its polymer precursor, J. Therm. Anal. Calorim. 134 (2018) 933–939, https://doi.org/10.1007/s10973-018-7318-4.

[24] E. Li, L. Liao, G. Lv, Z. Li, C. Yang, Y. Lu, The Interactions Between Three Typical PPCPs and LDH , Frontiers in Chemistry . 6 (2018) 16. https://www.frontiersin.org/article/10.3389/fchem.2018.00016.

[25] J. Wang, X. Guo, Adsorption kinetic models: physical meanings, applications, and solving methods, J. Hazard. Mater. 390 (2020), https://doi.org/10.1016/J.JHAZMAT.2020.122156 122156.

[26] E.K. Putra, R. Pranowo, J. Sunarso, N. Indraswati, S. Ismadji, Performance of activated carbon and bentonite for adsorption of amoxicillin from wastewater: mechanisms, isotherms and kinetics, Water Res. 43 (2009) 2419–2430, https://doi.org/10.1016/J.WATRES.2009.02.039.

[27] M.A. Al-Ghouti, D.A. Da'ana, Guidelines for the use and interpretation of adsorption isotherm models: A review, Journal of Hazardous Materials. 393 (2020) 122383, doi: https://doi.org/10.1016/J.JHAZMAT.2020.122383.

[28] A.F. Belhaj, K.A. Elraies, M.S. Alnarabiji, F.A. Abdul Kareem, J.A. Shuhli, S.M. Mahmood, H. Belhaj, Experimental investigation, binary modelling and artificial neural network prediction of surfactant adsorption for enhanced oil recovery application, Chem. Eng. J. 406 (2021), https://doi.org/10.1016/J.CEJ.2020.127081 127081.

[29] G.M. Hutchins, O.A. Anaya, Measurements of cardiac size, chamber volumes and valve orifices at autopsy, Johns Hopkins Med. J. 106 (1973) 133.

[30] M. Jafari, M.R. Rahimi, A. Asfaram, M. Ghaedi, H. Javadian, Experimental design for the optimization of paraquat removal from aqueous media using a fixed-bed column packed with Pinus Eldarica stalks activated carbon, Chemosphere (2021) 132670, https://doi.org/10.1016/j.chemosphere.2021.132670.

[31] H. Bolbol, M. Fekri, M. Hejazi-Mehrizi, Layered double hydroxide–loaded biochar as a sorbent for the removal of aquatic phosphorus: behavior and mechanism insights, Arabian J. Geosci. 12 (2019) 503, https://doi.org/10.1007/s12517-019-4694-4.

[32] G. Mitran, T. Cacciaguerra, S. Loridant, D. Tichit, I.C. Marcu, Oxidative dehydrogenation of propane over cobalt-containing mixed oxides obtained from LDH precursors, Appl. Catal. A: General 417–418 (2012) 153–162, https://doi.org/10.1016/J.APCATA.2011.12.038.

[33] F. Cavani, F. Trifirò, A. Vaccari, Hydrotalcite-type anionic clays: preparation, properties and applications, Catal. Today 11 (1991) 173–301, https://doi.org/10.1016/0920-5861(91)80068-K.

[34] M.M. Rao, B.R. Reddy, M. Jayalakshmi, V.S. Jaya, B. Sridhar, Hydrothermal synthesis of Mg–Al hydrotalcites by urea hydrolysis, Mater. Res. Bull. 40 (2005) 347–359, https://doi.org/10.1016/J.MATERRESBULL.2004.10.007.

[35] R. Pourfaraj, S.J. Fatemi, S.Y. Kazemi, P. Biparva, Synthesis of hexagonal mesoporous MgAl LDH nanoplatelets adsorbent for the effective adsorption of Brilliant Yellow, J. Colloid Interface Sci. 508 (2017) 65–74, https://doi.org/10.1016/J.JCIS.2017.07.101.

[36] A. Elhalil, M. Farnane, A. Machrouhi, F.Z. Mahjoubi, R. Elmoubarki, H. Tounsadi, M. Abdennouri, N. Barka, Effects of molar ratio and calcination temperature on

the adsorption performance of Zn/Al layered double hydroxide nanoparticles in the removal of pharmaceutical pollutants, J. Sci.: Adv. Mater. Devices 3 (2018) 188–195, https://doi.org/10.1016/J.JSAMD.2018.03.005.

[37] M. Khitous, Z. Salem, D. Halliche, Removal of phosphate from industrial wastewater using uncalcined MgAl-NO3 layered double hydroxide: batch study and modeling, Desalin. Water Treat. 57 (2016) 15920–15931, https://doi.org/10.1080/19443994.2015.1077745.

[38] K. Parida, L. Mohapatra, Recent progress in the development of carbonate-intercalated Zn/Cr LDH as a novel photocatalyst for hydrogen evolution aimed at the utilization of solar light, Dalton Trans. 41 (2012) 1173–1178, https://doi.org/10.1039/C1DT10957J.

[39] H. Xu, S. Zhu, M. Xia, F. Wang, Rapid and efficient removal of diclofenac sodium from aqueous solution via ternary core-shell CS@PANI@LDH composite: Experimental and adsorption mechanism study, Journal of Hazardous Materials. 402 (2021) 123815, doi: https://doi.org/10.1016/j.jhazmat.2020.123815.

[40] F.L. Theiss, G.A. Ayoko, R.L. Frost, Thermogravimetric analysis of selected layered double hydroxides, J. Therm. Anal. Calorim. 112 (2013) 649–657, https://doi.org/10.1007/s10973-012-2584-z.

[41] H. Luo, Y. Zhang, Y. Xie, Y. Li, M. Qi, R. Ma, S. Yang, Y. Wang, Iron-rich microorganism-enabled synthesis of magnetic biocarbon for efficient adsorption of diclofenac from aqueous solution, Bioresour. Technol. 282 (2019) 310–317, https://doi.org/10.1016/J.BIORTECH.2019.03.028.

[42] A. Llinàs, J.C. Burley, K.J. Box, R.C. Glen, J.M. Goodman, Diclofenac solubility: independent determination of the intrinsic solubility of three crystal forms, J. Med. Chem. 50 (2007) 979–983, https://doi.org/10.1021/jm0612970.

[43] C. Saucier, M.A. Adebayo, E.C. Lima, R. Cataluña, P.S. Thue, L.D.T. Prola, M.J. Puchana-Rosero, F.M. Machado, F.A. Pavan, G.L. Dotto, Microwave-assisted activated carbon from cocoa shell as adsorbent for removal of sodium diclofenac and nimesulide from aqueous effluents, J. Hazard. Mater. 289 (2015) 18–27, https://doi.org/10.1016/J.JHAZMAT.2015.02.026.

[44] L. Santamaría, M. López-Aizpún, M. García-Padial, M.A. Vicente, S.A. Korili, A. Gil, Zn-Ti-Al layered double hydroxides synthesized from aluminum saline slag wastes as efficient drug adsorbents, Appl. Clay Sci. 187 (2020), https://doi.org/10.1016/J.CLAY.2020.105486 105486.

[45] N. Fiol, I. Villaescusa, Determination of sorbent point zero charge: usefulness in sorption studies, Environ. Chem. Lett. 7 (2009) 79–84, https://doi.org/10.1007/s10311-008-0139-0.

[46] Y. Seida, Y. Nakano, Removal of phosphate by layered double hydroxides containing iron, Water Res. 36 (2002) 1306–1312, https://doi.org/10.1016/S0043-1354(01)00340-2.

[47] C. Novillo, D. Guaya, A. Allen-Perkins Avendaño, C. Armijos, J.L. Cortina, I. Cota, Evaluation of phosphate removal capacity of Mg/Al layered double hydroxides from aqueous solutions, Fuel 138 (2014) 72–79, https://doi.org/10.1016/J.FUEL.2014.07.010.

[48] J. Wang, X. Guo, Adsorption isotherm models: classification, physical meaning, application and solving method, Chemosphere 258 (2020), https://doi.org/10.1016/J.CHEMOSPHERE.2020.127279 127279.

[49] A.L. Johnston, E. Lester, O. Williams, R.L. Gomes, Understanding Layered Double Hydroxide properties as sorbent materials for removing organic pollutants from environmental waters, Journal of Environmental Chemical Engineering. 9 (2021) 105197, doi: https://doi.org/10.1016/J.JECE.2021.105197.

[50] C. Jing, Y. Chen, X. Zhang, X. Guo, X. Liu, B. Dong, F. Dong, X. Zhang, Y. Liu, S. Li, Y. Zhang, Low carbonate contaminative and ultrasmall NiAl LDH prepared by acid salt treatment with high adsorption capacity of Methyl Orange, Ind. Eng. Chem. Res. 58 (2019) 11985–11998, https://doi.org/10.1021/acs.iecr.9b01706.

[51] Y. Zhao, F. Liu, X. Qin, Adsorption of diclofenac onto goethite: adsorption kinetics and effects of pH, Chemosphere 180 (2017) 373–378, https://doi.org/10.1016/J.CHEMOSPHERE.2017.04.007.

[52] P. Kumari, B. Pal, R.K. Das, Superior adsorptive removal of eco-toxic drug diclofenac sodium by Zn–Al LDH·xBi2O3 layer double hydroxide composites, Appl. Clay Sci. 208 (2021), https://doi.org/10.1016/J.CLAY.2021.106119 106119.

[53] S. Radmehr, M. Hosseini Sabzevari, M. Ghaedi, M.H. Ahmadi Azqhandi, F. Marahel, Adsorption of nalidixic acid antibiotic using a renewable adsorbent based on Graphene oxide from simulated wastewater, Journal of Environmental Chemical Engineering. 9 (2021) 105975, doi: https://doi.org/10.1016/J.JECE.2021.105975.

[54] Y. Liu, Y.J. Liu, Biosorption isotherms, kinetics and thermodynamics, Sep. Purif. Technol. 61 (2008) 229–242, https://doi.org/10.1016/J.SEPPUR.2007.10.002.

[55] K. Gupta, J.B. Huo, J.C.E. Yang, M.L. Fu, B. Yuan, Z. Chen, (MoS4)2− intercalated CAMoS4·LDH material for the efficient and facile sequestration of antibiotics from aqueous solution, Chem. Eng. J. 355 (2019) 637–649, https://doi.org/10.1016/J.CEJ.2018.08.200.

[56] G. Crini, P.M. Badot, Application of chitosan, a natural aminopolysaccharide, for dye removal from aqueous solutions by adsorption processes using batch studies: A review of recent literature, Prog. Polym. Sci. 33 (2008) 399–447, https://doi.org/10.1016/J.PROGPOLYMSCI.2007.11.001.

[57] P. Saha, S. Chowdhury, Thermodynamics, InTech, 2011.

[58] P. Saha, S. Chowdhury, S. Gupta, I. Kumar, Insight into adsorption equilibrium, kinetics and thermodynamics of Malachite Green onto clayey soil of Indian origin, Chemical Engineering Journal 165 (2010) 874–882, https://doi.org/10.1016/j.cej.2010.10.048.

[59] L. Liang, L. Li, Adsorption behavior of calcined layered double hydroxides towards removal of iodide contaminants, J. Radioanal. Nucl. Chem. 273 (2007) 221–226, https://doi.org/10.1007/s10967-007-0740-x.

[60] K.-H. Goh, T.-T. Lim, Z. Dong, Application of layered double hydroxides for removal of oxyanions: a review, Water Res. 42 (2008) 1343–1368, https://doi.org/10.1016/j.watres.2007.10.043.

[61] R. Zăvoianu, R. Bîrjega, E. Angelescu, O.D. Pavel, Effect of hydration temperature on the structure reconstruction of MgAlY layered materials, C. R. Chim. 21 (2018) 318–326, https://doi.org/10.1016/J.CRCI.2017.07.002.

[62] R. Han, Y. Wang, X. Zhao, Y. Wang, F. Xie, J. Cheng, M. Tang, Adsorption of methylene blue by phoenix tree leaf powder in a fixed-bed column: experiments and prediction of breakthrough curves, Desalination 245 (2009) 284–297, https://doi.org/10.1016/J.DESAL.2008.07.013.

[63] X.F. Sun, T. Imai, M. Sekine, T. Higuchi, K. Yamamoto, A. Kanno, S. Nakazono, Adsorption of phosphate using calcined Mg3–Fe layered double hydroxides in a fixed-bed column study, J. Ind. Eng. Chem. 20 (2014) 3623–3630, https://doi.org/10.1016/J.JIEC.2013.12.057.